Supplementary Materials for

Improving efficiency and stability of perovskite solar cells with photocurable fluoropolymers

Federico Bella,* Gianmarco Griffini,* Juan-Pablo Correa-Baena, Guido Saracco, Michael Grätzel, Anders Hagfeldt,* Stefano Turri, Claudio Gerbaldi

*Corresponding author. Email: federico.bella@polito.it (F.B.); gianmarco.griffini@polimi.it (G.G.); anders.hagfeldt@epfl.ch (A.H.)

Published 29 September 2016 on *Science* First Release
DOI: 10.1126/science.aah4046

This PDF file includes:

1. Materials and Methods

Preparation and characterization of perovskite solar cells

Electron selective layer preparation. Nippon Sheet Glass 10 Ω/sq was cleaned by sonication in 2% Hellmanex water solution for 30 min. After rinsing with deionised water and ethanol, substrates were further cleaned by UV ozone treatment for 15 min. Then, a compact layer of TiO_2 (50-70 nm thick) was deposited on FTO via spray pyrolysis at 450 °C from a precursor solution of titanium diisopropoxide bis(acetylacetonate) in anhydrous ethanol. After spraying, substrates were kept at 450 °C for 45 min and left to cool down to ambient temperature. Then, a mesoporous TiO_2 layer was deposited by spin coating for 20 s at 4000 rpm with a ramp of 2000 rpm s^{-1}, using 30 nm particle paste (30 NR-D, Dyesol) diluted in ethanol to obtain a 150-200 nm thick layer. After spin coating, substrates were immediately dried at 100 °C for 10 min and then sintered again at 450 °C for 30 min under dry air flow.

Lithium ion doping of mesoporous TiO_2 was achieved by spin coating a 0.10 M solution of bis(trifluoromethane)sulfonimide lithium salt (LiTFSI, Sigma Aldrich) in acetonitrile (*28*). The solution was prepared freshly before the application under nitrogen atmosphere: 50 µl were poured on 1.4 × 2.4 cm^2 substrate. Li^+-treated electrodes were completed with a second calcination step at 450 °C for 30 min. After cooling down to 150 °C, substrates were immediately transferred in a glove box (MBraun Labstar 100) under controlled nitrogen atmosphere for depositing the perovskite films.

Perovskite precursor solution and film preparation. Perovskite films were deposited from a precursor solution containing formamidinium iodide (FAI, 1.0 M, Sigma Aldrich), PbI_2 (1.1 M, TCI Chemicals), methylammonium bromide (MABr, 0.20 M,

Sigma Aldrich) and $PbBr_2$ (0.22 M, AlfaAesar) in anhydrous DMF:DMSO 4:1 (v:v, Acros). The perovskite solution was spin-coated in a two-step program: first at 1000 rpm for 10 s and then at 6000 rpm for 30 s. During the second step, 100 μL of chlorobenzene were poured on the spinning substrate 15 s prior to the end of the program to form smooth films of perovskite by rapid crystallisation. Substrates were then annealed at 100 °C for 1 h in the nitrogen-filled glove box.

The spiro-OMeTAD (Merck) solution (70 mM in chlorobenzene) was spun at 4000 rpm for 20 s. The spiro-OMeTAD was doped at a molar ratio of 0.50, 0.030 and 3.3 with LiTFSI), tris(2-(1H-pyrazol-1-yl)-4-tert-butylpyridine)-cobalt(III) tris(bis(trifluoromethylsulfonyl)imide) (FK209, Dyenamo) and 4-tert-butylpyridine (TBP, Sigma Aldrich), respectively (*13*). As a last step, 70-80 nm of gold top electrode were thermally evaporated under high vacuum.

Solar cells characterization. A ZEISS Merlin HR-SEM was used to characterize the morphology of the device cross-section. The solar cell performance was measured using a 450 W Xenon light source (Oriel) and the spectral mismatch between AM1.5G and the simulated illumination was reduced by the use of a Schott K113 Tempax filter (Präzisions Glas & Optik GmbH). The light intensity was calibrated with a Si photodiode equipped with an IR-cutoff filter (KG3, Schott) and recorded during each measurement. *J-V* characteristics of the solar cells were obtained by applying an external potential bias while measuring the current response using a digital source meter (Keithley 2400). The potential scan rate was 5 mV s^{-1} and no device preconditioning was applied before starting the measurement, such as light soaking or forward potential bias applied for long time. The starting potential was determined as the potential at which the solar cells provided 1 mA in forward bias, no equilibration time was used.

Solar cells were covered with a black metal mask limiting the active area to 0.16 cm^2 and reducing the influence of the scattered light. The IPCE spectra were measured in DC mode by chopping at 2 Hz a monochromatic light generated by a 300 W Xenon lamp (ICL Technology); a Gemini-180 double-monochromator with 1200 grooves per mm grating (Jobin Yvon Ltd) and a lock-in amplifier (SR830 DSP, Stanford Research System) completed the IPCE setup.

Aging tests were carried out following three different protocols (see **Fig. S1**) on batches of 5 solar cells each. In the first aging test, solar cells were kept in an Ar-filled dry glove box (MBraun Labstar, O_2 and H_2O content <0.1 ppm) and irradiated (8 h per day) with a UV optical fiber (5 mW cm^{-2}, Lightningcure LC8, Hamamatsu) for 3 months; then, solar cells were placed in a quartz chamber with constant relative humidity (RH = 50%) and the aging test proceeded for other 3 months always under UV irradiation. In this protocol (6 months total duration), PCE was measured once a week. The second aging test was carried out by placing (without any coverage) the PSCs on the terrace of the Politecnico di Torino building in Turin (45°06'N, 7°66'E), and monitoring their PV parameters under 1 sun irradiation once a week for a period of 3 months. For the third aging experiment, a batch of 5 solar cells was placed around a beaker filled with boiling water and kept at 105 °C on a hot plate; solar cells were placed on a thermally insulating support to avoid overheating due to contact with the hot plate. The whole system was then covered with a glass bell to generate a ≈100% humidity environment (measured RH: 95%) on the five devices. The experiment was performed for 1 month, measuring the performance of the solar cells once a week and refilling water in the beaker whenever necessary.

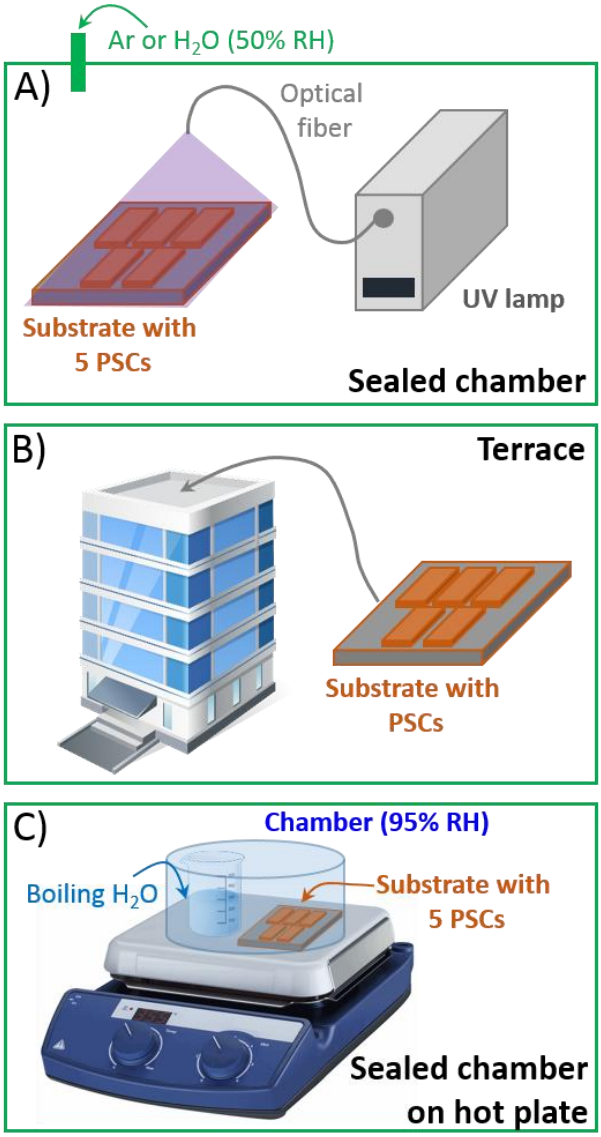

Fig. S1. Sketched representation of the series of setups developed for aging experiments of PSCs: (**A**) Devices are kept in a chamber filled with Ar or kept at 50% RH, under 5 mW cm^{-2} of UV irradiation; (**B**) Devices are placed on the terrace of the Politecnico di Torino building in Turin; (**C**) Devices are placed under a sealed chamber on a thermal insulator positioned above a hot plate heating up a water-filled beaker to produce boiling water.

Preparation and characterization of the fluoropolymeric coatings

The photocurable fluoropolymeric coating (UV-coating) used as host matrix material for front and back coverage of the PSC stack was obtained starting from a formulation developed recently in our laboratories for application on photoelectrochromic devices (*25*). In detail, a UV-curable fluoropolymeric binder based on a chloro-trifluoro-ethylene vinyl ether resin (Lumiflon LF-910LM, Asahi Glass Corporation (*34*)) was mixed with a difunctional methacrylic perfluoropolyether oligomer (Fluorolink MD700, Solvay Specialty Polymers) in the 98:2 weight ratio, followed by dilution with $CHCl_3$ (30 wt% total dry content). Irgacure 1173 (BASF) was added (3 wt%) as radical photoinitiator. For the fabrication of the LDS coating, Lumogen F Violet 570 (BASF, in this work referred to as V570) was added to the polymer solution in different amounts (0.5-3 wt%). Prior to deposition, the precursor formulation was mixed under magnetic stirring overnight under dark conditions. To obtain the final solid fluoropolymer coating, the precursor formulation was deposited on the PSC device (on the outer face of the FTO substrate in the case of dye-doped LDS coatings – front coverage; on top of the gold back contact in the case of undoped UV-coating – back coverage) by spin coating (1000 rpm, 30 s on a SPIN150 spin coater, SPS-Europe) in the nitrogen-filled glove box, followed by UV-curing by means of a medium pressure mercury lamp equipped with an optical guide (Lightningcure LC8, Hamamatsu) for 60 s under an irradiation intensity of 25 mW cm^{-2} (measured with the Power Puck II radiometer). The so-obtained fluoropolymeric coatings were 5 μm thick, as measured by optical profilometry (Microfocus, UBM).

To avoid any unexpected damage of the thin gold back contact film during fluoropolymer deposition, the UV-curable precursor solution was dispensed under

controlled glove box environment on the back contact side of the PSC device while the substrate was spinning. This deposition technique allowed promoting swift evaporation of the solvent from the fluoropolymeric formulation thus avoiding deterioration of the metallic film and subsequent worsening of device performance. Formation of the solid film was achieved by UV-curing the as-cast material following the same procedure used for the formation of the LDS coating. To ensure external electrical contacts, copper tape lined with an acrylic conductive adhesive was used prior to fluoropolymer deposition.

Differential scanning calorimetry (DSC) was employed to evaluate the glass transition temperature (T_g) of the crosslinked coating material, by means of a Mettler-Toledo DSC/823e instrument at a scan rate of 20 °C min^{-1} under N_2 flux. Values of T_g were obtained from the second heating ramp. The thermal stability of the UV-coating was evaluated by means of thermo-gravimetric analysis (TGA) on fully crosslinked solid state samples with a Q500 TGA system (TA Instruments) operated from ambient temperature to 800 °C at a scan rate of 10 °C min^{-1} both in air and under flowing N_2. The surface wetting behaviour of the fluoropolymeric coatings was evaluated at ambient temperature by means of an optical contact angle measuring apparatus (OCA 20, Data Physics) equipped with a CCD photocamera and a 500 μL Hamilton syringe to dispense liquid droplets. Water (H_2O) and diiodomethane (CH_2I_2) were used as probe liquids. The optical absorption characteristics of the fluoropolymeric coatings were investigated by collecting the UV-Vis absorption spectra of spin-coated solid films at increasing fluorophore concentration in air at ambient temperature in transmission mode with an Evolution 600 UV-Vis spectrophotometer (Thermo Scientific). Similarly, fluorescence emission spectra were obtained in air at ambient temperature by using a Jasco FP-6600 Spectrofluorometer. The excitation wavelength for the V570-doped LDS coatings was

350 nm. X-ray diffraction (XRD) measurements were performed on solid films by means of a Bruker D8 Advance X-ray diffractometer using a Cu Kα source, a step size of 0.02° and an acquisition time of 0.5 deg min^{-1}. In order to avoid interference given by the presence of the Au top film, adhesive tape was used to gently delaminate it. The presence of spiro-OMeTAD did not affect the XRD measurement of the inner perovskite layer because of its amorphous nature.

2. Optical properties of the LDS coatings

To investigate the effect of the concentration of fluorophore hosted in the fluoropolymeric matrix on the optical properties of the LDS coating, absorption and emission spectra of the LDS layer at increasing dye concentrations were collected on 5 μm thick UV-coatings, as shown in **Fig. S2A-B**. As expected, a progressive increase in dye concentration leads to a correspondingly increased absorption intensity (absorbance). However, for high dye concentrations (> 2 wt%), negative deviations are observed from the linearity predicted by the Beer-Lambert law of absorption, which directly correlates the absorbance to the chromophore concentration (see **Fig. S2C**). This behavior likely suggests a limited solubility of the dye in the UV-coating host matrix at such high dye loadings. Indeed, the very low solubility parameter of fluorinated and perfluorinated polymeric materials combined with the poor miscibility of these systems in common organic solvents limits largely their thermodynamic miscibility with organic dyes in high concentrations.

Contrary to what is found for the absorption spectra, the fluorescence emission intensity displays a maximum for 2 wt% dye concentration, above which a progressive decrease is observed (2.5-3 wt% dye concentration) (**Fig. S2B**). To investigate thoroughly this effect, the peak emission intensity was plotted as a function of the peak absorbance for UV-coatings at increasing dye concentrations. As shown in **Fig. S2D**, a steady increase in the emission intensity with absorbance is observed for absorption intensities up to 0.9 (2 wt% dye concentration). However, higher absorbance values (*viz.*, dye concentrations > 2 wt%) result in a sharp decrease of the peak emission intensity, thus indicating that for heavily doped UV-coatings dissipative processes may come into play causing partial loss of the absorbed photons. In this respect, high dye

concentrations in the UV-coatings (> 2 wt%) may lead to fluorescence quenching due to aggregate formation (*35*,*36*) and to decreased photoluminescence quantum yields as a result of the formation of low-energy electronic states (e.g., dimers, excimers) acting as optical traps for fluorescence photons (*37*). Accordingly, 2 wt% dye concentration may represent a threshold value above which such dissipative processes start to significantly influence the optical response of the UV-coatings. A concurrent effect responsible for the observed decrease in the emission intensity at high luminophore concentrations in the UV-coating may be associated with the partial overlap between absorption and emission spectra of the fluorescent dye. In this respect, a higher dye concentration (i.e., a coating with higher optical density) implies a high probability for emitted photons to be re-absorbed by other adjacent dye molecules, thus limiting the fluorescence through the LDS coating due to re-absorption losses. In the system presented here, such effect is found to be relevant for dye concentrations exceeding 2 wt% (*38*).

It is interesting to note that increasing the dye concentration in the LDS coating also leads to a progressive red shift of the fluorescence emission peak (inset to **Fig. S2B**), which is not observed in the corresponding absorption spectra (inset to **Fig. S2A**). Such 5 nm bathochromic shift (λ_{max}(em) of 430 and 435 nm for UV-coatings doped with 0.5 and 3 wt% dye concentrations, respectively) may be correlated with two parallel effects taking place in the coatings at increasing dye concentrations. On the one hand, the progressively higher fluorophore concentrations in the coating result in higher optical density. This determines an increasingly shorter distance between adjacent dye molecules that, in turn, leads to the (re)emission of second (and higher) generation fluorescence photons characterized by gradually longer emission wavelengths. On the other hand, aggregate formation becomes increasingly more relevant as the

concentration of the dye is increased, as previously discussed. Because such aggregates may exhibit red-shifted spectral response (both absorption and emission) if compared to single dye molecules (*39*), they can be excited by second-generation photons emitting at longer wavelengths, thus leading to progressively red-shifted emission spectra. Being the probability of experiencing aggregate formation in the coating directly correlated with dye concentration, this effect is increasingly more pronounced as the concentration of the dye increases.

Considering the data listed in **Table 1**, the only solar cells showing worsened PCE values compared to the pristine device were those laden with fluorophore in the 0-0.5 wt% range. In particular, these solar cells showed a lower J_{sc} with respect to the uncoated devices. Such lower performance can be ascribed to the partial penetration into the device stack of UV rays emitted from the Hg lamp used for the photopolymerization of the coating on the front electrode. The detrimental effect of the high-energy component of the solar spectrum on the perovskite layer is well known in the literature (*10−12*), and such low dye concentrations cannot ensure their complete absorption. Likewise, the UV-absorbing radical photoinitiator present in the reactive mixture is not able to provide sufficient shielding effect. This problem was not experimented for V570 concentrations higher than 0.5%.

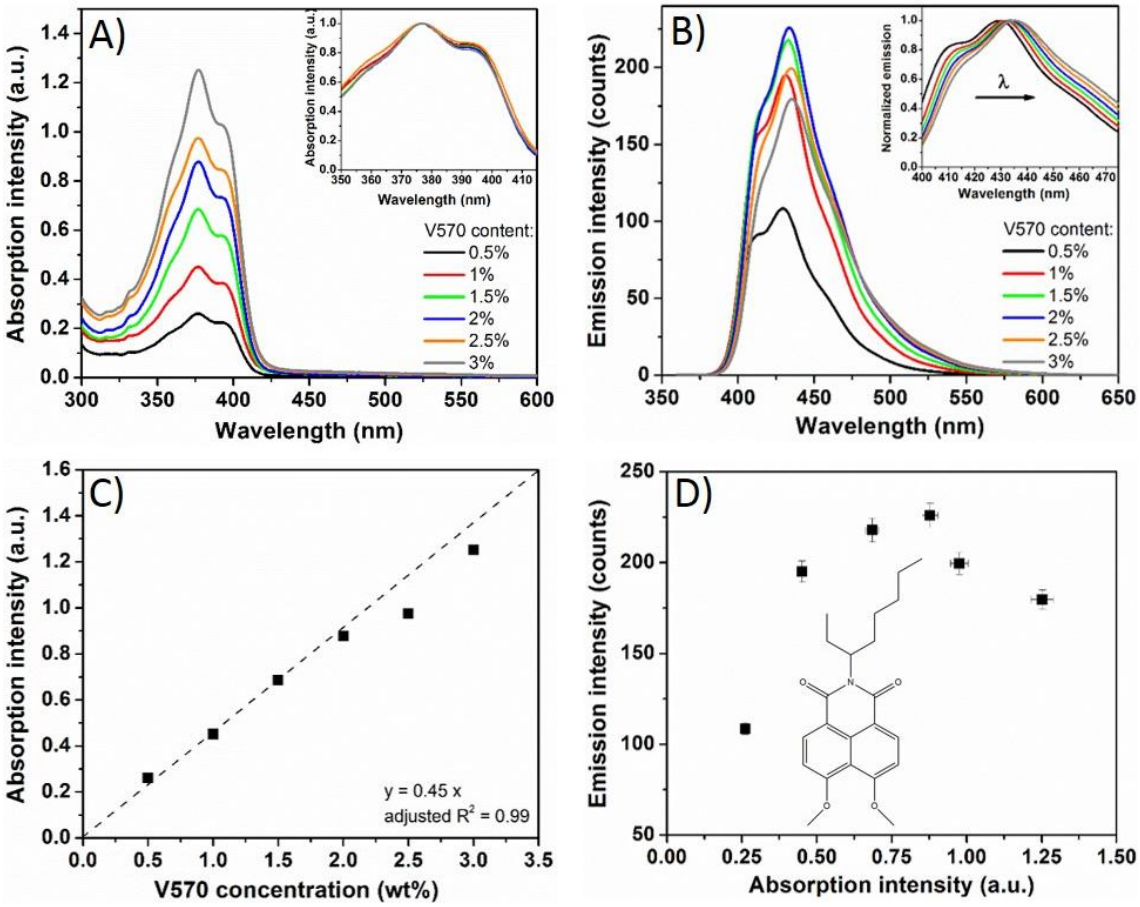

Fig. S2. A) UV-VIS absorption and **B)** Fluorescent emission spectra of UV-coatings at increasing fluorophore concentration (insets show a zoom of the absorption and emission peaks); **C)** Plot of absorbance *vs.* chromophore concentration for the LDS fluorinated coating developed in this work loaded with increasing concentrations of V570. For dye concentrations exceeding 2 wt%, negative deviations from the linearity predicted by the Beer-Lambert law are observed (dashed line and corresponding equation are shown in the plot); **D)** Fluorescence peak emission intensity *vs.* UV-vis peak absorption intensity for UV-coatings with increasing dye concentrations (error bars represent deviations from the mean values measured on five different samples); inset: chemical structure of V570.

3. Surface wettability behavior of the LDS coatings

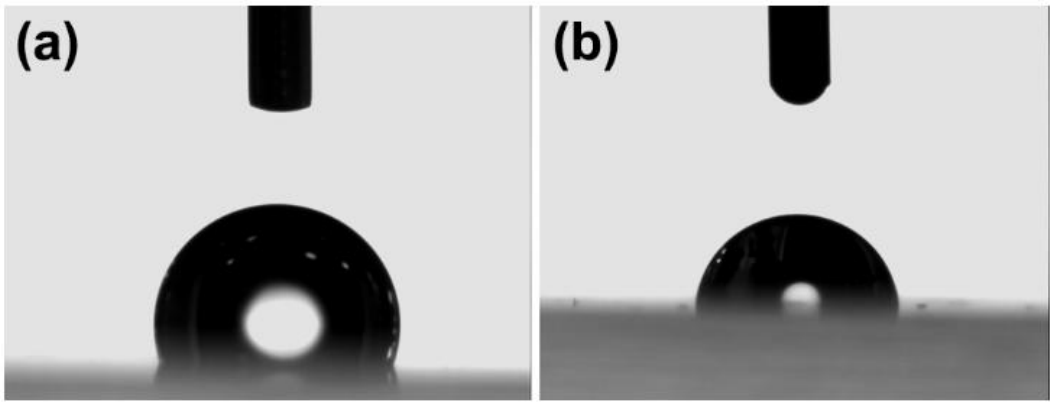

Fig. S3. Optical contact angle measurements of **(a)** water (111°) and **(b)** diiodomethane (91°) on the fluoropolymeric crosslinked coating. The resulting surface energy of the coating is $\gamma = 18$ mN m^{-1} (polar component $\gamma_p = 2.7$ mN m^{-1}, dispersive component $\gamma_d = 15.3$ mN m^{-1}).

4. Thermal properties of the LDS coatings

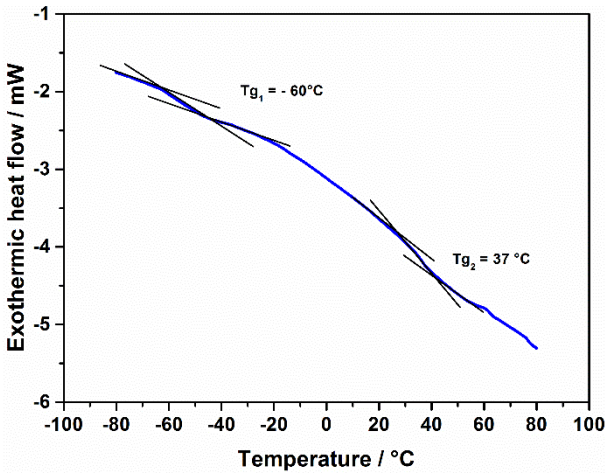

Fig. S4. DSC trace of the fluoropolymeric crosslinked coating. Two glass transition temperatures (T_g) can be clearly distinguished, ascribed to the nanoscale biphasic nature of the perfluorinated component of the coating. T_{g1} (− 60 °C) is attributed to the soft fluorinated segments, while T_{g2} (37 °C) is associated to the hard hydrogenated urethane phase.

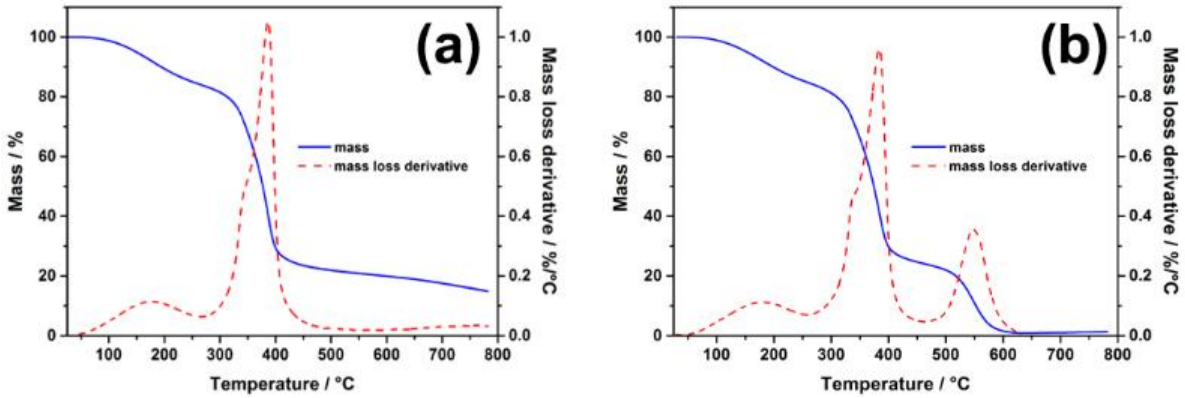

Fig. S5. TGA thermograms of the fluorinated crosslinked coating carried out **(a)** in nitrogen atmosphere and **(b)** in air.

5. Variation of photovoltaic parameters during aging test

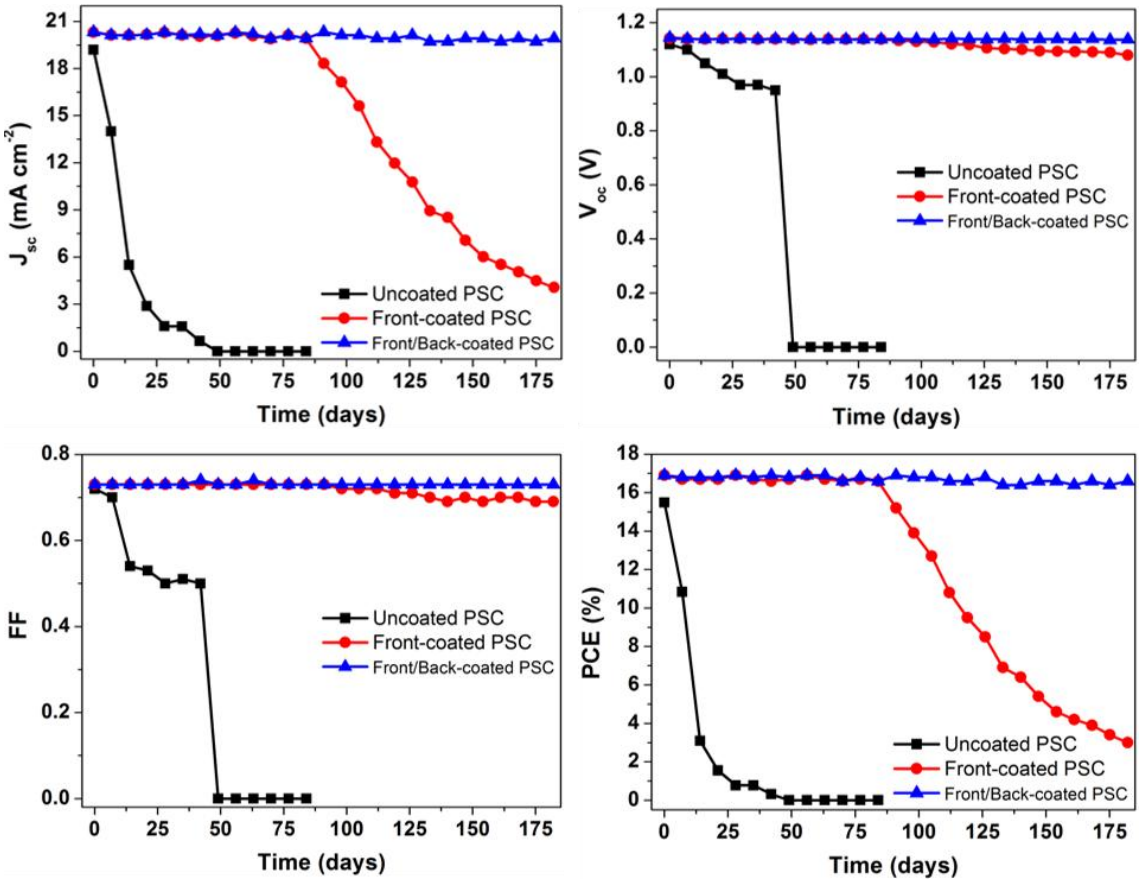

Fig. S6. Evolution of averaged PV parameters of PSCs reported in **Fig. 4A**. The experiment consisted of an aging test on the three series of PSCs: uncoated, front-coated (i.e., luminescent fluorinated coating on the front-side), and front/back coated (i.e., front-side coated with the luminescent fluorophore and back contact coated with the moisture-resistant fluoropolymeric layer). During the first 3 months, PSCs were kept under Ar atmosphere, while in the next 3 months under air at 50% RH, in both cases under continuous UV irradiation. PCE was measured once a week.

6. Comments on XRD patterns in Fig. 4B

In order to elucidate the mechanisms behind the stability of front/back-coated PSC devices, XRD analysis was performed on both uncoated and coated (front and front/back) samples after the aging test and the results were compared with the pristine system (**Fig. 4B**). In addition to the typical reflections associated with the perovskite material (*16,40*), the pristine coating exhibits some peaks related to unreacted residual PbI_2, as expected from the excess PbI_2 used for the production of the perovskite material (*27,28*). Upon aging, structural changes are observed in terms of appearance of additional diffraction peaks as well as modifications of the relative peak intensities. Upon continuous exposure to UV light in inert atmosphere, uncoated samples exhibit a increase in the intensity of the 12.7° signal, which is characteristic of the (001) plane of PbI_2. In addition, an evident decrease is found of the relative intensity of the peaks referred to perovskite at 20.2°, 40.8° and 43.3°. These trends suggest partial decomposition of the crystalline perovskite material into PbI_2, with the simultaneous presence of both phases. Upon exposure to humid environment, the relative intensity of the signal at 12.7° becomes predominant with respect to all other peaks referred to the perovskite material, thus accounting for conversion to PbI_2. In addition, other peaks related to the PbI_2 phase appear at 25.7°, 38.8° and 52.5°, typical of the (011), (110), (004) plane reflections, respectively. These changes clearly reflect the well-known sensitivity of perovskites to moisture penetrating from the back-side of the solar cell stack and leading to the degradation of the material, which in turn leads to device performance decay. In these conditions, the UV-shielding effect ensured by the presence of the fluorinated LDS coating on the external side of the FTO glass substrate does not prove to be sufficient to avoid the observed moisture-induced degradation

pathways. Conversely, the front/back-coated PSC configuration effectively prevents water to infiltrate the device owing to the additional presence of the highly hydrophobic fluorinated coating deposited on the back-side of the PSC stack that acts as water-impermeable protective barrier. As evidenced by the XRD pattern of the front/back-coated system, no significant modifications are observed even after extended exposure to high relative humidity in a sealed environment, ultimately highlighting the effectiveness of the proposed strategy in guaranteeing stable device efficiency over the entire accelerated aging test.

7. Outdoor aging test carried out in summer

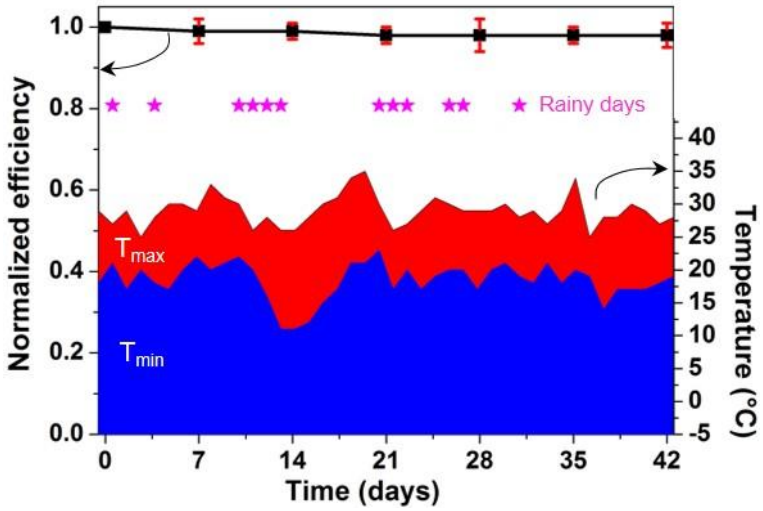

Fig. S7. Results of the summer aging test on front/back coated devices left for 5 weeks on the terrace of the Politecnico di Torino building in Turin (Italy), thus experiencing real outdoor operating conditions in warm season (1st July – 12th August, 2016). PCE was measured once a week. A batch 5 solar cells was subjected to highly variable climatic conditions, as outdoor temperatures ranged from +11 to +35 °C, and 12 days over 42 were characterized by summer storms (*33*).

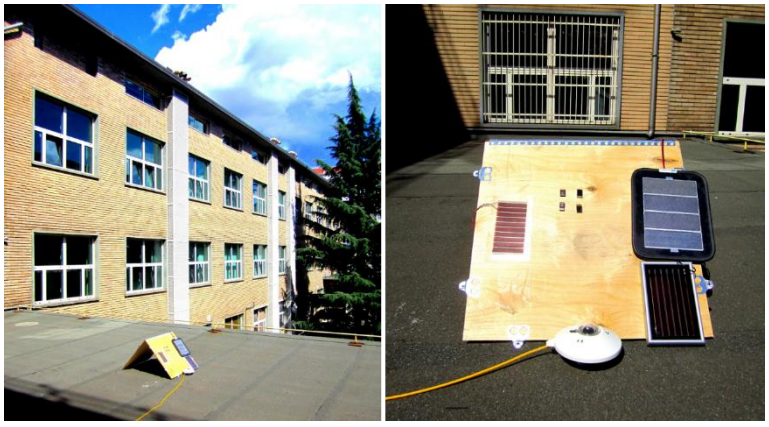

Fig. S8. Setup on the terrace of the Politecnico di Torino building in Turin for solar cells aging studies. The platform hosts a few PV devices currently under investigation, and PSCs are placed in the middle of the exposed area (4 solar cells in the picture, the fifth one was under *J*-*V* measurement in the solar cells lab).

References

1. H. S. Kim, C. R. Lee, J. H. Im, K. B. Lee, T. Moehl, A. Marchioro, S. J. Moon, R. Humphry-Baker, J. H. Yum, J. E. Moser, M. Grätzel, N. G. Park, Lead iodide perovskite sensitized all-solid-state submicron thin film mesoscopic solar cell with efficiency exceeding 9%. *Sci. Rep.* **2**, 591 (2012).

2. M. M. Lee, J. Teuscher, T. Miyasaka, T. N. Murakami, H. J. Snaith, Efficient hybrid solar cells based on meso-superstructured organometal halide perovskites. *Science* **338**, 643–647 (2012).doi:10.1126/science.1228604 Medline

3. H. Zhou, Q. Chen, G. Li, S. Luo, T. B. Song, H. S. Duan, Z. Hong, J. You, Y. Liu, Y. Yang, Interface engineering of highly efficient perovskite solar cells. *Science* **345**, 542–546 (2014).doi:10.1126/science.1254050 Medline

4. M. Liu, M. B. Johnston, H. J. Snaith, Efficient planar heterojunction perovskite solar cells by vapour deposition. *Nature* **501**, 395–398 (2013).doi:10.1038/nature12509 Medline

5. J. Burschka, N. Pellet, S. J. Moon, R. Humphry-Baker, P. Gao, M. K. Nazeeruddin, M. Grätzel, Sequential deposition as a route to high-performance perovskite-sensitized solar cells. *Nature* **499**, 316–319 (2013).doi:10.1038/nature12340 Medline

6. National Center for Photovoltaics (NCPV) at the National Renewable Energy Laboratory (NREL); http://www.nrel.gov/ncpv (accessed July 2016).

7. N. G. Park, Perovskite solar cells: An emerging photovoltaic technology. *Mater. Today* **18**, 65–72 (2015). doi:10.1016/j.mattod.2014.07.007

8. J. Seo, J. H. Noh, S. I. Seok, Rational strategies for efficient perovskite solar cells. *Acc. Chem. Res.* **49**, 562–572 (2016).doi:10.1021/acs.accounts.5b00444 Medline

9. H. S. Jung, N. G. Park, Perovskite solar cells: From materials to devices. *Small* **11**, 10–25 (2015).doi:10.1002/smll.201402767 Medline

10. T. A. Berhe, W. N. Su, C. H. Chen, C. J. Pan, J. H. Cheng, H. M. Chen, M. C. Tsai, L. Y. Chen, A. A. Dubale, B. J. Hwang, Organometal halide perovskite solar cells: Degradation and stability. *Energy Environ. Sci.* **9**, 323–356 (2016). doi:10.1039/C5EE02733K

11. Y. Rong, L. Liu, A. Mei, X. Li, H. Han, Beyond efficiency: The challenge of stability in mesoscopic perovskite solar cells. *Adv. Energy Mater.* **5**, 1501066 (2015). doi:10.1002/aenm.201501066

12. T. Leijtens, G. E. Eperon, N. K. Noel, S. N. Habisreutinger, A. Petrozza, H. J. Snaith, Stability of metal halide perovskite solar cells. *Adv. Energy Mater.* **5**, 1500963 (2015). doi:10.1002/aenm.201500963

13. J. P. Correa Baena, L. Steier, W. Tress, M. Saliba, S. Neutzner, T. Matsui, F. Giordano, T. J. Jacobsson, A. R. Srimath Kandada, S. M. Zakeeruddin, A. Petrozza, A. Abate, M. K. Nazeeruddin, M. Grätzel, A. Hagfeldt, Highly efficient planar perovskite solar cells through band alignment engineering. *Energy Environ. Sci.* **8**, 2928–2934 (2015). doi:10.1039/C5EE02608C

14. J. P. Correa-Baena, M. Anaya, G. Lozano, W. Tress, K. Domanski, M. Saliba, T. Matsui, T. J. Jacobsson, M. E. Calvo, A. Abate, M. Grätzel, H. Míguez, A. Hagfeldt, Unbroken

perovskite: Interplay of morphology, electro-optical properties, and ionic movement. *Adv. Mater.* **28**, 5031–5037 (2016).doi:10.1002/adma.201600624 Medline

15. H. C. Weerasinghe, Y. Dkhissi, A. D. Scully, R. A. Caruso, Y. B. Cheng, Encapsulation for improving the lifetime of flexible perovskite solar cells. *Nano Energy* **18**, 118–125 (2015). doi:10.1016/j.nanoen.2015.10.006

16. I. Hwang, I. Jeong, J. Lee, M. J. Ko, K. Yong, Enhancing stability of perovskite solar cells to moisture by the facile hydrophobic passivation. *ACS Appl. Mater. Interfaces* **7**, 17330–17336 (2015).doi:10.1021/acsami.5b04490 Medline

17. M. Kaltenbrunner, G. Adam, E. D. Głowacki, M. Drack, R. Schwödiauer, L. Leonat, D. H. Apaydin, H. Groiss, M. C. Scharber, M. S. White, N. S. Sariciftci, S. Bauer, Flexible high power-per-weight perovskite solar cells with chromium oxide-metal contacts for improved stability in air. *Nat. Mater.* **14**, 1032–1039 (2015).doi:10.1038/nmat4388 Medline

18. J. You, L. Meng, T.-B. Song, T.-F. Guo, Y. M. Yang, W.-H. Chang, Z. Hong, H. Chen, H. Zhou, Q. Chen, Y. Liu, N. De Marco, Y. Yang, Improved air stability of perovskite solar cells via solution-processed metal oxide transport layers. *Nat. Nanotechnol.* **11**, 75–81 (2016).doi:10.1038/nnano.2015.230 Medline

19. K. Domanski, J. P. Correa-Baena, N. Mine, M. K. Nazeeruddin, A. Abate, M. Saliba, W. Tress, A. Hagfeldt, M. Grätzel, Not all that glitters is gold: Metal-migration-induced degradation in perovskite solar cells. *ACS Nano* **10**, 6306–6314 (2016).doi:10.1021/acsnano.6b02613 Medline

20. X. Li, M. I. Dar, C. Yi, J. Luo, M. Tschumi, S. M. Zakeeruddin, M. K. Nazeeruddin, H. Han, M. Grätzel, Improved performance and stability of perovskite solar cells by crystal crosslinking with alkylphosphonic acid ω-ammonium chlorides. *Nat. Chem.* **7**, 703–711 (2015).doi:10.1038/nchem.2324 Medline

21. A. Mei, X. Li, L. Liu, Z. Ku, T. Liu, Y. Rong, M. Xu, M. Hu, J. Chen, Y. Yang, M. Grätzel, H. Han, A hole-conductor-free, fully printable mesoscopic perovskite solar cell with high stability. *Science* **345**, 295–298 (2014).doi:10.1126/science.1254763 Medline

22. L. Zhang, T. Liu, L. Liu, M. Hu, Y. Yang, A. Mei, H. Han, The effect of carbon counter electrodes on fully printable mesoscopic perovskite solar cells. *J. Mater. Chem. A* **3**, 9165–9170 (2015). doi:10.1039/C4TA04647A

23. W. Li, W. Zhang, S. Van Reenen, R. J. Sutton, J. Fan, A. A. Haghighirad, M. B. Johnston, L. Wang, H. J. Snaith, Enhanced UV-light stability of planar heterojunction perovskite solar cells with caesium bromide interface modification. *Energy Environ. Sci.* **9**, 490–498 (2016). doi:10.1039/C5EE03522H

24. Materials and methods are available as supplementary materials on *Science* Online.

25. F. Bella, G. Leftheriotis, G. Griffini, G. Syrrokostas, S. Turri, M. Grätzel, C. Gerbaldi, A new design paradigm for smart windows: Photocurable polymers for quasi-solid photoelectrochromic devices with excellent long-term stability under real outdoor operating conditions. *Adv. Funct. Mater.* **26**, 1127–1137 (2016). doi:10.1002/adfm.201503762

26. L. R. Wilson, B. S. Richards, Measurement method for photoluminescent quantum yields of fluorescent organic dyes in polymethyl methacrylate for luminescent solar concentrators. *Appl. Opt.* **48**, 212–220 (2009).doi:10.1364/AO.48.000212 Medline

27. D. Bi, W. Tress, M. I. Dar, P. Gao, J. Luo, C. Renevier, K. Schenk, A. Abate, F. Giordano, J. P. Correa Baena, J.-D. Decoppet, S. M. Zakeeruddin, M. K. Nazeeruddin, M. Grätzel, A. Hagfeldt, Efficient luminescent solar cells based on tailored mixed-cation perovskites. *Sci. Adv.* **2**, e1501170 (2016).doi:10.1126/sciadv.1501170 Medline

28. F. Giordano, A. Abate, J. P. Correa Baena, M. Saliba, T. Matsui, S. H. Im, S. M. Zakeeruddin, M. K. Nazeeruddin, A. Hagfeldt, M. Graetzel, Enhanced electronic properties in mesoporous TiO_2 via lithium doping for high-efficiency perovskite solar cells. *Nat. Commun.* **7**, 10379 (2016).doi:10.1038/ncomms10379 Medline

29. D. Liu, T. L. Kelly, Perovskite solar cells with a planar heterojunction structure prepared using room-temperature solution processing techniques. *Nat. Photonics* **8**, 133–138 (2014). doi:10.1038/nphoton.2013.342

30. J.-H. Im, I.-H. Jang, N. Pellet, M. Grätzel, N.-G. Park, Growth of $CH_3NH_3PbI_3$ cuboids with controlled size for high-efficiency perovskite solar cells. *Nat. Nanotechnol.* **9**, 927–932 (2014).doi:10.1038/nnano.2014.181 Medline

31. G. Griffini, M. Levi, S. Turri, Novel crosslinked host matrices based on fluorinated polymers for long-term durability in thin-film luminescent solar concentrators. *Sol. Energy Mater. Sol. Cells* **118**, 36–42 (2013). doi:10.1016/j.solmat.2013.05.041

32. G. Griffini, M. Levi, S. Turri, Novel high-durability luminescent solar concentrators based on fluoropolymer coatings. *Prog. Org. Coat.* **77**, 528–536 (2014). doi:10.1016/j.porgcoat.2013.11.016

33. Il Meteo; http://www.ilmeteo.it/meteo/Torino (accessed June 2016).

34. G. Griffini, F. Bella, F. Nisic, C. Dragonetti, D. Roberto, M. Levi, R. Bongiovanni, S. Turri, Multifunctional luminescent down-shifting fluoropolymer coatings: A straightforward strategy to improve the UV-light harvesting ability and long-term outdoor stability of organic dye-sensitized solar cells. *Adv. Energy Mater.* **5**, 1401312 (2015). doi:10.1002/aenm.201401312

35. C. Haines, M. Chen, K. P. Ghiggino, The effect of perylene diimide aggregation on the light collection efficiency of luminescent concentrators. *Sol. Energy Mater. Sol. Cells* **105**, 287–292 (2012). doi:10.1016/j.solmat.2012.06.030

36. F. Bella, G. Griffini, M. Gerosa, S. Turri, R. Bongiovanni, Performance and stability improvements for dye-sensitized solar cells in the presence of luminescent coatings. *J. Power Sources* **283**, 195–203 (2015). doi:10.1016/j.jpowsour.2015.02.105

37. H. Yoo, J. Yang, A. Yousef, M. R. Wasielewski, D. Kim, Excimer formation dynamics of intramolecular π-stacked perylenediimides probed by single-molecule fluorescence spectroscopy. *J. Am. Chem. Soc.* **132**, 3939–3944 (2010).doi:10.1021/ja910724x Medline

38. G. Griffini, M. Levi, S. Turri, Thin-film luminescent solar concentrators: A device study towards rational design. *Renew. Energy* **78**, 288–294 (2015). doi:10.1016/j.renene.2015.01.009

39. R. O. Al-Kaysi, T. Sang Ahn, A. M. Müller, C. J. Bardeen, The photophysical properties of chromophores at high (100 mM and above) concentrations in polymers and as neat solids. *Phys. Chem. Chem. Phys.* **8**, 3453–3459 (2006).doi:10.1039/B605925B Medline

40. J. A. Christians, P. A. Miranda Herrera, P. V. Kamat, Transformation of the excited state and photovoltaic efficiency of $CH_3NH_3PbI_3$ perovskite upon controlled exposure to humidified air. *J. Am. Chem. Soc.* **137**, 1530–1538 (2015).doi:10.1021/ja511132a Medline